Gene Symbol	Assay ID	Gene Symbol	Assay ID
1. GAPDH	Hs99999905_m1	25. LIFR	Hs00158730_m1
2. CCNA2	Hs00996788_m1	26. CD164	Hs00985280_m1
3. TGFB1	Hs00998133_m1	27. SIGLEC1	Hs00988063_m1
4. TGFB2	Hs01548875_m1	28. KDR	Hs00176676_m1
5. TGFB3	Hs01086000_m1	29. PPARG	Hs00234592_m1
6. ENG	Hs00923996_m1	30. BMPR1B	Hs00176144_m1
7. MCAM	Hs00174838_m1	31. PTCH1	Hs00970979_m1
8. ITGB1	Hs01127543_m1	32. GLI1	Hs00171790_m1
9. CD44	Hs01075861_m1	33. GLI2	Hs01119973_m1
10. THY1	Hs00174816_m1	34. GLI3	Hs00609233_m1
11. NGFR	Hs00609976_m1	35. SMO	Hs01090242_m1
12. ANPEP	Hs00174265_m1	36. SP7	Hs00541729_m1
13. ALCAM	Hs00233455_m1	37. BMPR2	Hs00176148_m1
14. CD34	Hs02576480_m1	38. COL1A1	Hs00164004_m1
15. KIT	Hs00174029_m1	39. MSX2	Hs00741177_m1
16. CD14	Hs00169122_m1	40. OCN	Hs00609452_g1
17. CD68	Hs00154355_m1	41. BMPR1A	Hs01034912_g1
18. CD163	Hs00174705_m1	42. RUNX2	Hs01047976_m1
19. GGT1	Hs00980756_m1	43. ALPL	Hs01029144_m1
20. MFI2	Hs00195551_m1	44. BMP1	Hs00196183_m1
21. ABCB1	Hs00184500_m1	45. BMP2	Hs01055564_m1
22. FZD9	Hs00268954_s1	46. BMP4	Hs00370078_m1
23. SEMA4D	Hs00396705_m1	47. BMP5	Hs00234930_m1
24. PVRL1	Hs00161050_m1	48. BMP7	Hs00233476_m1

Table S1. TaqMan gene expression assays used for single cell transcription analysis.

Gene Name	Forward primer sequence (5' to 3')	Reverse primer sequence (5' to 3')
Osteogenic genes		
ALP, human	ATGGGATGGGTGTCTCCACA	CCACGAAGGGGAACTTGTC
BMP2, human	ACCCGCTGTCTTCTAGCGT	CTCAGGACCTCGTCAGAGGG
BMP4, human	TTCCTGGTAACCGAATGCTGA	CCCTGAATCTCGGCGACTTTT
BMPR1B, human	CTTTTGCGAAGTGCAGGAAAAT	TGTTGACTGAGTCTTCTGGACAA
COL1a1, human	ATGACTATGAGTATGGGGAAGCA	TGGGTCCCTCTGTTACACTTT
ENG, human	AGCCCCACAAGTCTTGCAG	GCTAGTGGTATATGTCACCTCGC
GAPDH, human	ATGGGGAAGGTGAAGGTCG	GGGGTCATTGATGGCAACAATA
OCN, human	CACTCCTCGCCCTATTGGC	CCCTCCTGCTTGGACACAAAG
RUNX2, human	ATTCCTGTAGATCCGAGCACC	GCTCACGTCGCTCATTTTGC
Adipogenic Genes		
AP2, human	CCAGGGACTTTGGGTACGTG	GGTTGAGAAATTCAGCTACTGCT
GCP1, human	GCTTTCTGGGTGGACTCAAGT	TCTAGTGTCTCTGTGAGGACTG
LPL, human	TCATTCCCGGAGTAGCAGAGT	GGCCACAAGTTTTGGCACC
PPARγ, human	CCTATTGACCCAGAAAGCGATT	CATTACGGAGAGATCCACGGA

Table S2. Quantitative PCR Genes and Primer Sequences

Supplemental Figure 1

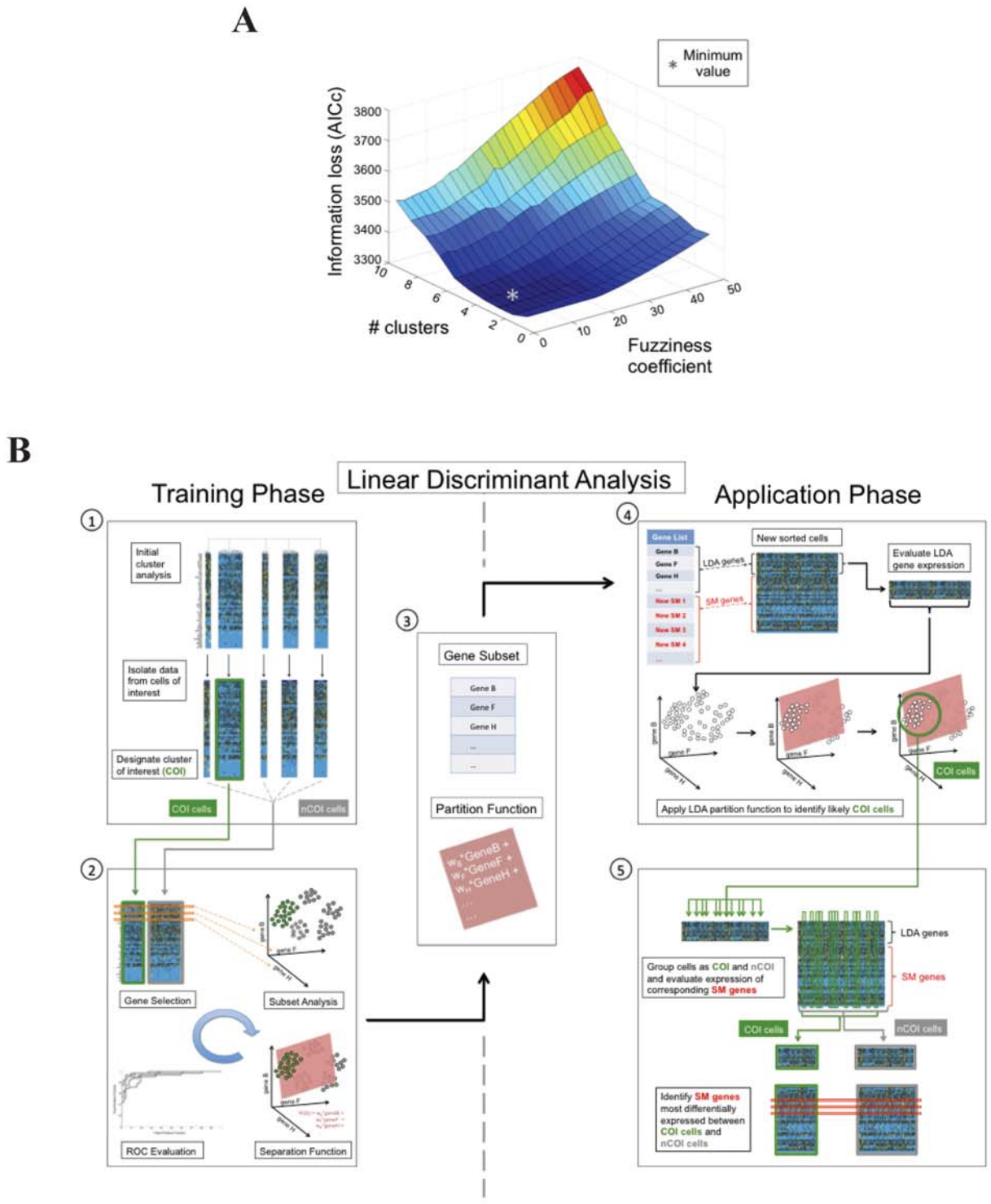

Fig. S1. ***Clustering algorithm for single cell transcriptional data.*** (A) Application of Akaike Information Criterion allows iterative determination of optimal clustering parameters to minimize theoretical information loss. An exhaustive approach is used to determine the information lost (z-axis) with different values for the number of clusters (y-axis) and the fuzziness coefficient (x-axis). The trough of this plot (asterisk) represents the optimal set of clustering parameters for a given data set. (B) Linear discriminate analysis schema. Dotted line denotes the separation between the training phase and the application phase.

Supplemental Figure 2

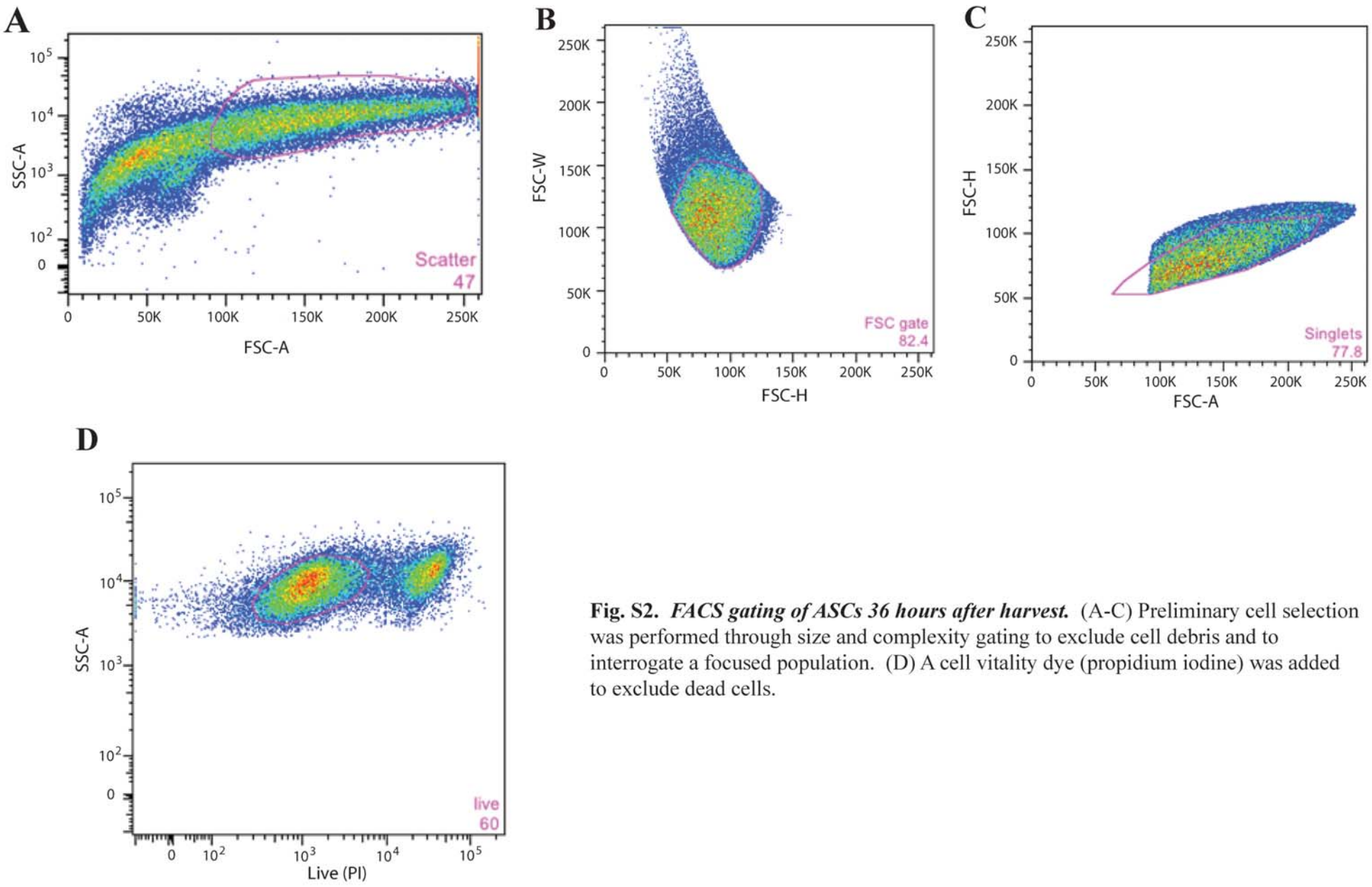

Fig. S2. ***FACS gating of ASCs 36 hours after harvest.*** (A-C) Preliminary cell selection was performed through size and complexity gating to exclude cell debris and to interrogate a focused population. (D) A cell vitality dye (propidium iodine) was added to exclude dead cells.

Supplemental Figure 3

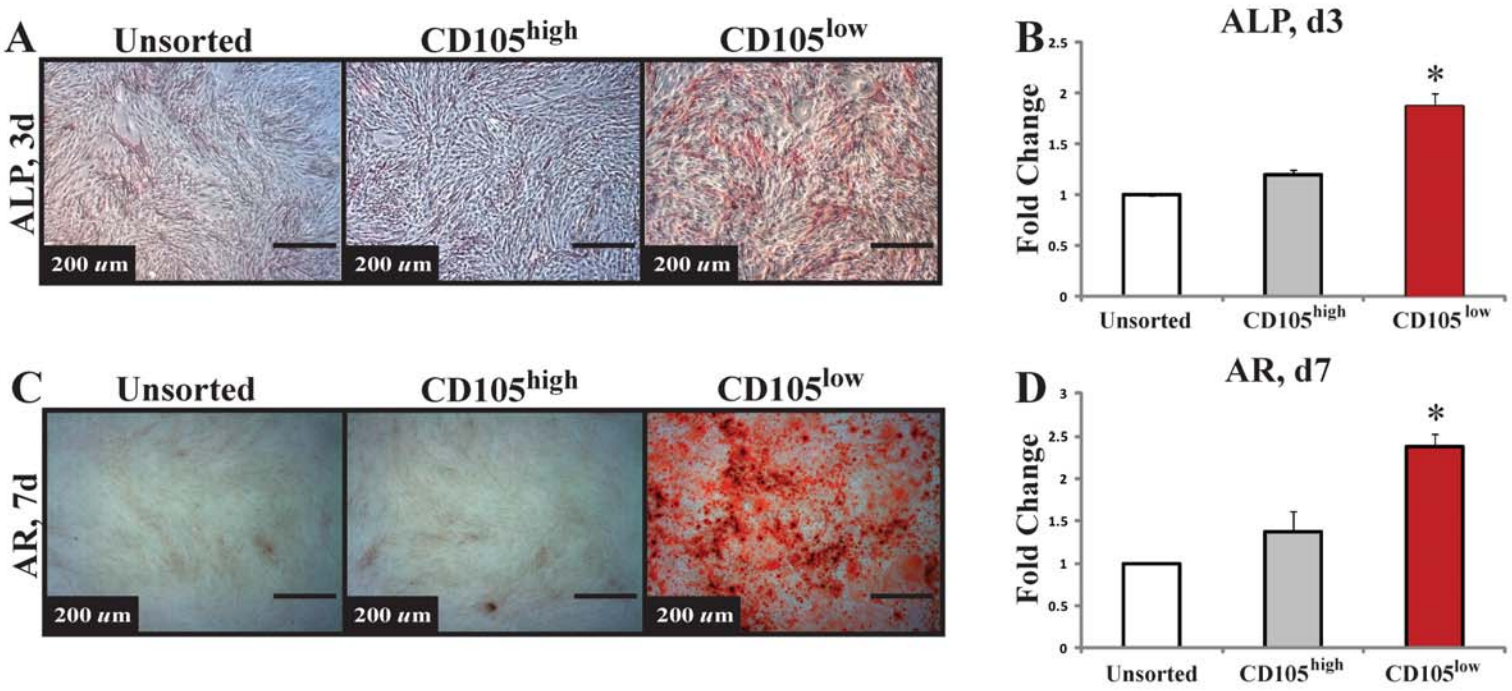

Fig. S3. ***Osteogenic Differentiation of Serum Starved sorted ASCs.*** (A) Alkaline phosphatase staining following three days of osteogenic differentiaiton. (B) Quantification of Alkaline phosphatase stain. (C) Alizarin red staining following seven days of osteogenic differentiation. (D) Quantification of Alizarin Red stain. Note despite cell-cyle synchronization prior to sort, $CD105^{low}$ ASCs continue to demonstrate enhanced osteogenesis relative to other groups.

Supplemental Figure 4

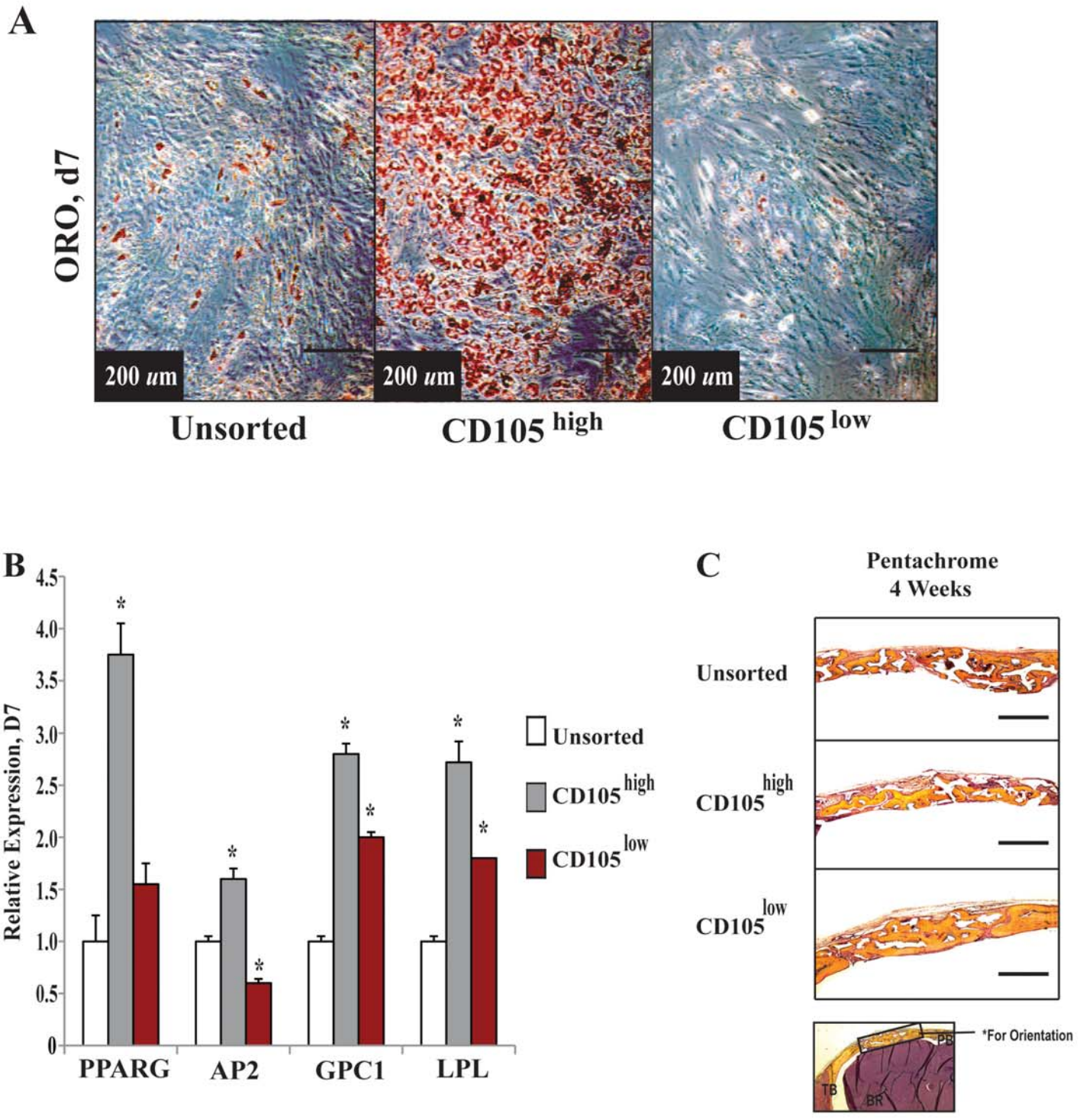

Fig. S4. ***Adipogenic and Chondrogenic Differentiation of sorted ASCs.*** (A) Oil red O staining showed enhanced adipogenic differentiation for CD105^{high} ASCs compared to unsorted and CD105^{low} cells. (B) Gene expression analysis confirmed histological staining, with the most significant upregulation of adipogenic genes among the CD105^{high} ASCs. (C) Pentachrome stain of critical-sized calvarial defects four weeks after treatment with the following:1) unsorted ASCs, 2) CD105^{high} ASCs and 3) CD105^{low} ASCs. Of note, there is absence of blue staining which would represent cartilage. Thus, the bone formed is likely due to intramembranous ossification.

Supplemental Figure 5

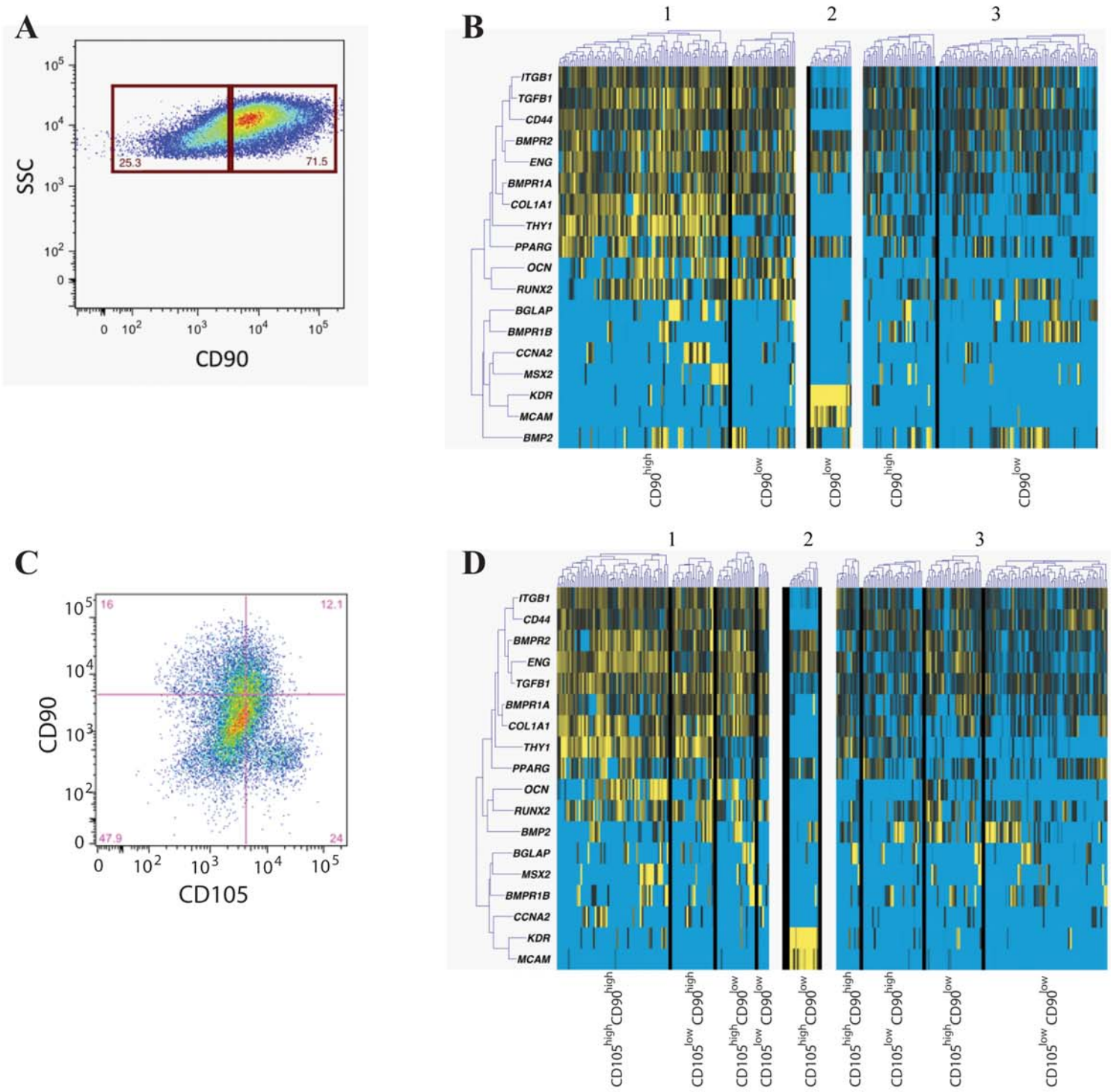

Fig. S5. ***FACS analysis and microfluidic-based single cell transcriptional characterization of CD90 single-sorted and CD105 CD90 double-sorted ASCs.*** (A) FACS analysis of CD90 expression 36 hours after ASC harvest. (B) Clustering of osteogenic gene expression data using an information theory-based algorithm (blinded to sorting parameters). Each cluster is further partitioned with respect to CD90 surface expression. (C) FACS analysis of joint CD105 and CD90 expression 36 hours after ASC harvest. (D) Partitioning of osteogenic gene clusters based on CD105 and CD90 expression demonstrating asymmetry in gene expression between each of the four groups ($CD105^{high}CD90^{high}$, $CD105^{low}CD90^{high}$, $CD105^{high}CD90^{low}$ and $CD105^{low}CD90^{low}$).

Supplemental Figure 6

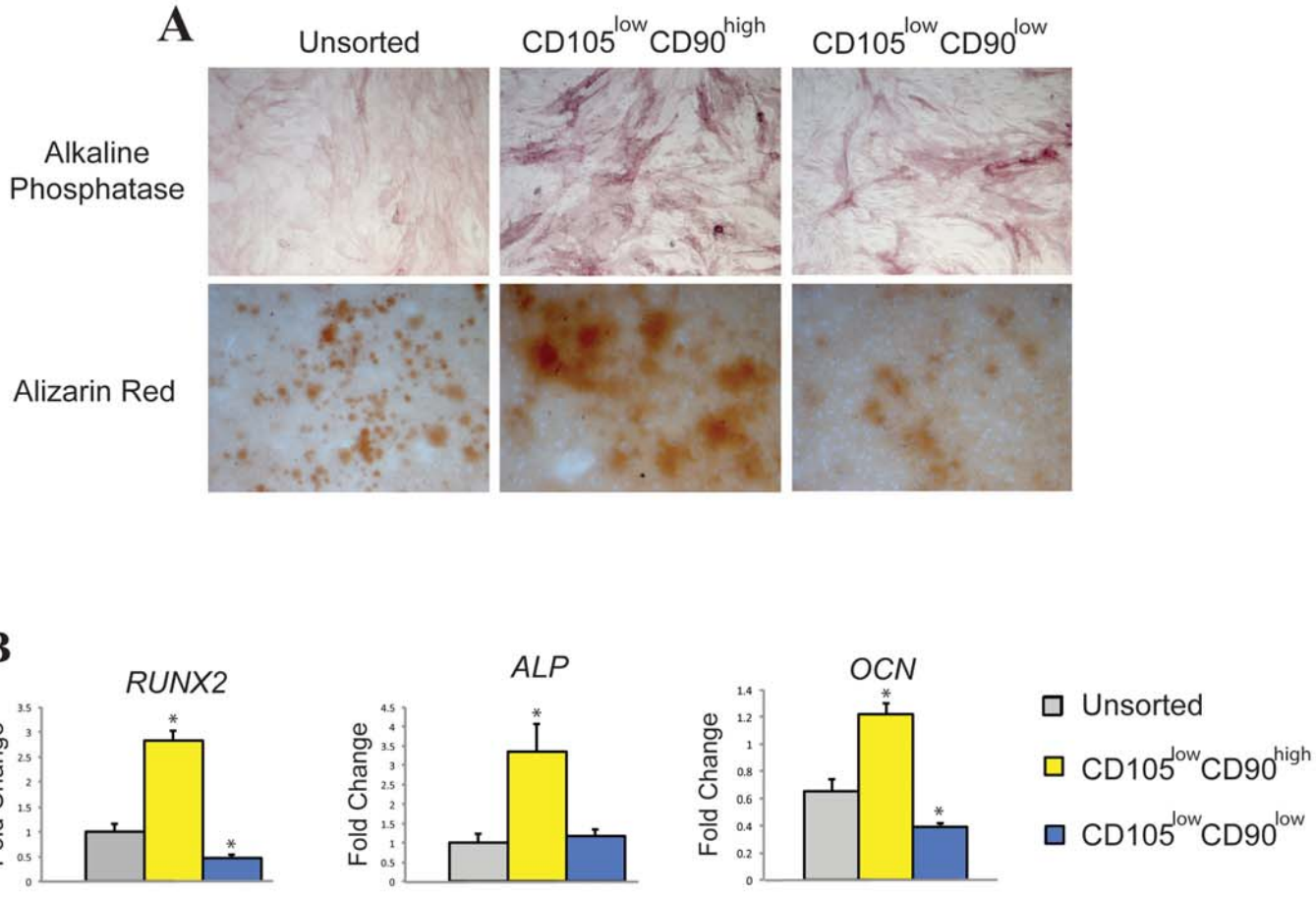

Fig. S6. ***Osteogenic Differentiation of CD105 CD90 double-sorted ASCs.*** (A) Alkaline Phosphatase and Alizarin Red stains of $CD105^{low}$ASCs that were either $CD90^{high}$ or $CD90^{low}$. (B) Osteogenic gene expression of unsorted, $CD105^{low}$ $CD90^{high}$and $CD105^{low}CD90^{low}$hASCs after three days in osteogenic medium (*RUNX2, ALP* and *OCN*).

Supplemental Figure 7

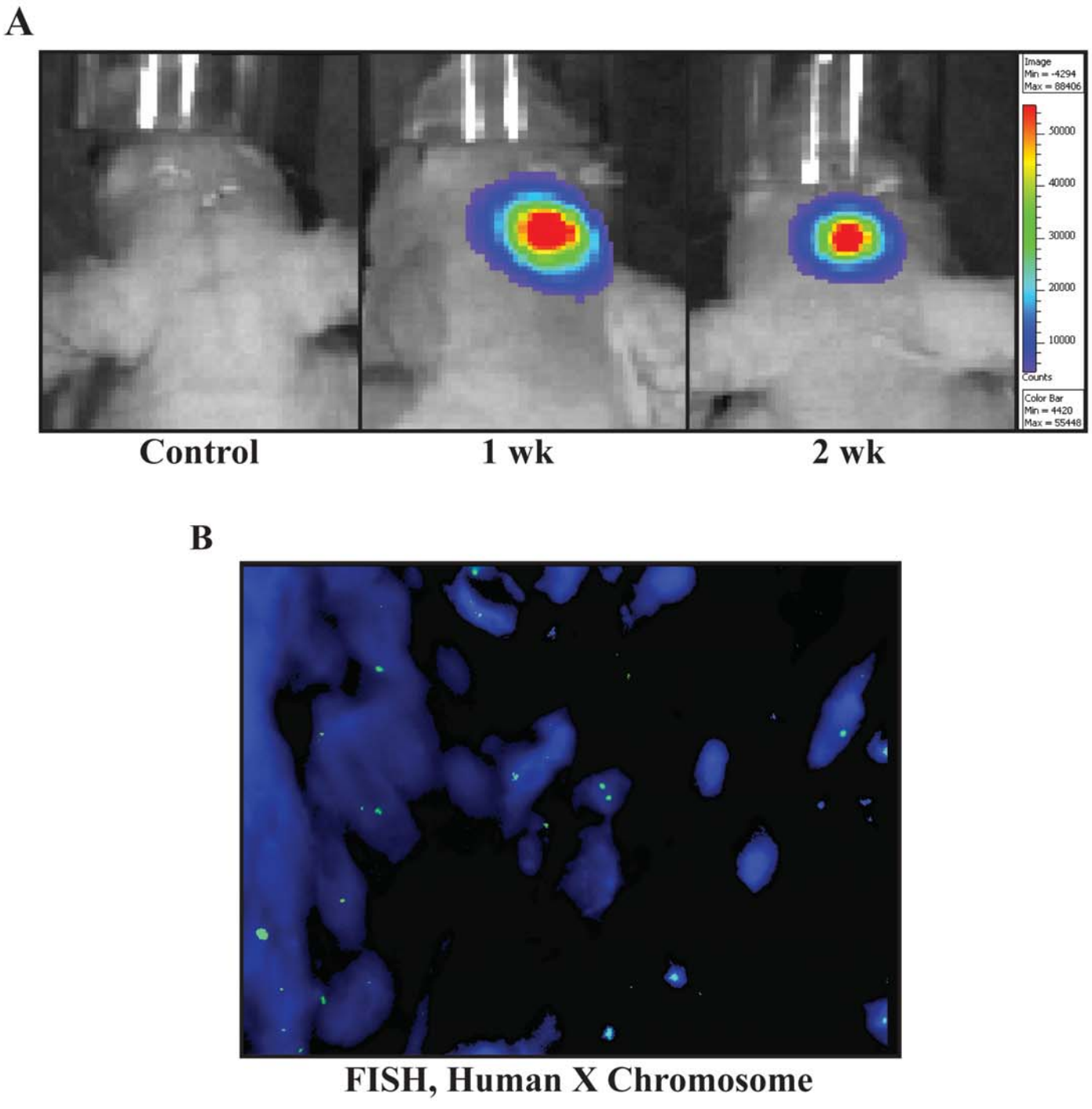

Fig. S7. ***Demonstration of cell persistence in vivo.*** (A) Luciferase activity in defects engrafted with Luc+ hASCs. Red represents the highest level of activity, followed by yellow, blue, dark blue, and purple. (B) Fluorescent *in situ* hybridization for human X chromosome, appearing green. DAPI nuclear counterstain appearing blue. As expected, many of the cells within the defect site at one week were of human origin, showing human X chromosomes. Specificity of FISH analysis was assessed, as sites other than the defect were negative (data not shown).

Supplemental Figure 8

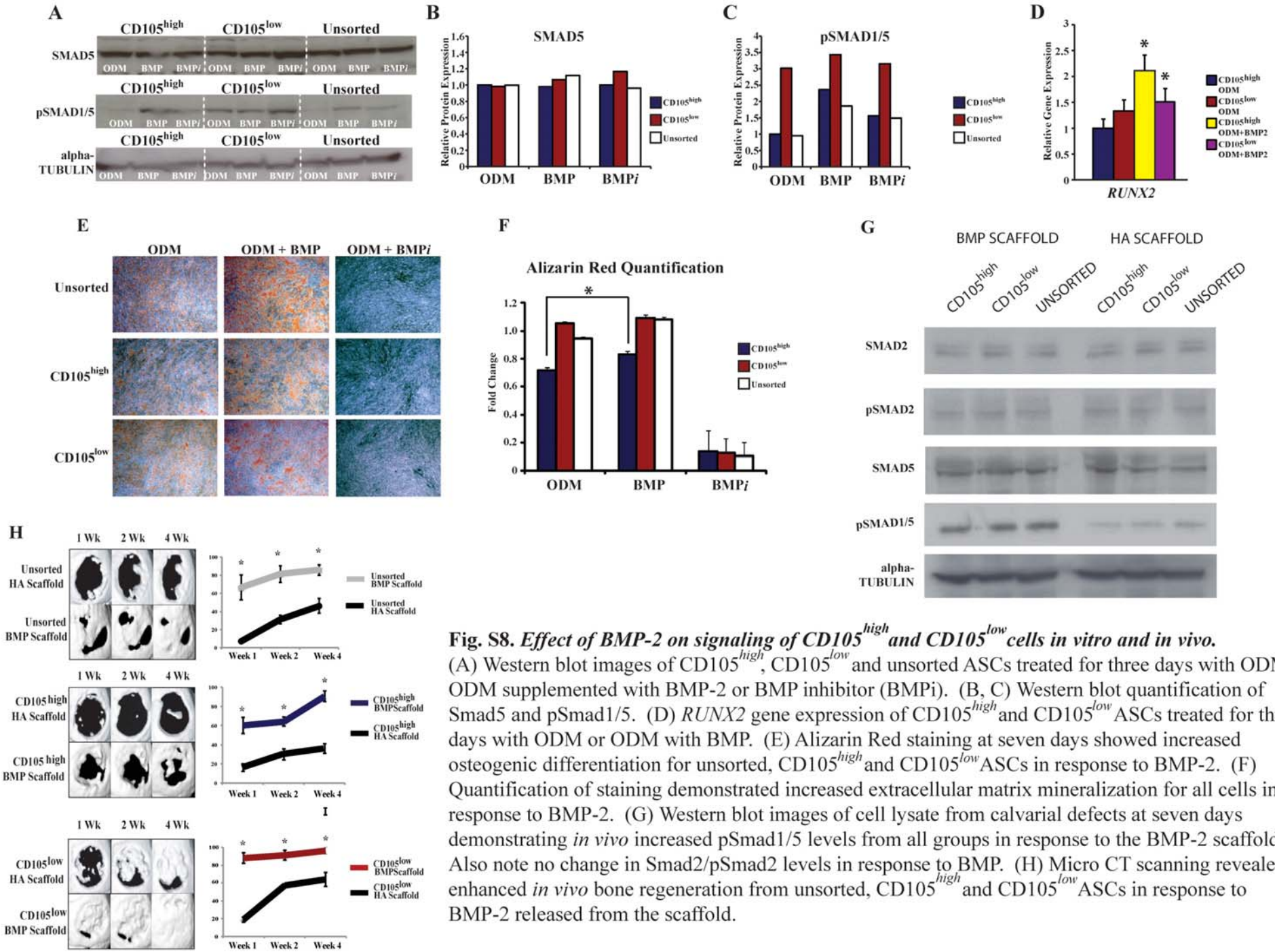

Fig. S8. ***Effect of BMP-2 on signaling of CD105^{high} and CD105^{low} cells in vitro and in vivo.*** (A) Western blot images of CD105^{high}, CD105^{low} and unsorted ASCs treated for three days with ODM, ODM supplemented with BMP-2 or BMP inhibitor (BMPi). (B, C) Western blot quantification of Smad5 and pSmad1/5. (D) *RUNX2* gene expression of CD105^{high} and CD105^{low} ASCs treated for three days with ODM or ODM with BMP. (E) Alizarin Red staining at seven days showed increased osteogenic differentiation for unsorted, CD105^{high} and CD105^{low} ASCs in response to BMP-2. (F) Quantification of staining demonstrated increased extracellular matrix mineralization for all cells in response to BMP-2. (G) Western blot images of cell lysate from calvarial defects at seven days demonstrating *in vivo* increased pSmad1/5 levels from all groups in response to the BMP-2 scaffold. Also note no change in Smad2/pSmad2 levels in response to BMP. (H) Micro CT scanning revealed enhanced *in vivo* bone regeneration from unsorted, CD105^{high} and CD105^{low} ASCs in response to BMP-2 released from the scaffold.